Earth Syst. Sci. Data Discuss., 5, 107–145, 2012
www.earth-syst-sci-data-discuss.net/5/107/2012/
doi:10.5194/essdd-5-107-2012

Open Access Earth System Science Data Discussions

Supraglacial dust and debris: geochemical compositions from glaciers in Svalbard, southern Norway, Nepal and New Zealand

K. A. Casey[1,*]

[1]NASA Goddard Space Flight Center, Cryospheric Sciences Laboratory, Code 615, Greenbelt, MD, 20771, USA
[*]formerly at: University of Oslo, Department of Geosciences, P.O. Box 1047 Blindern, 0316 Oslo, Norway

Received: 10 January 2012 – Accepted: 14 February 2012 – Published: 28 February 2012

Correspondence to: K. A. Casey (kimberly.a.casey@nasa.gov)

Published by Copernicus Publications.

Abstract

Alpine glacier samples were collected in four contrasting regions to measure supraglacial dust and debris geochemical composition and quantify regional variability. A total of 70 surface glacier ice, snow and debris samples were collected in Svalbard, southern Norway, Nepal and New Zealand. Trace elemental abundances in snow and ice samples were measured via inductively coupled plasma mass spectrometry (ICP-MS). Supraglacial debris mineral, bulk oxide and trace element composition were determined via X-ray diffraction (XRD) and X-ray fluorescence spectroscopy (XRF). A total of 45 major, trace and rare earth elements and 10 oxide compound abundances are reported. Elemental abundances revealed sea salt aerosol and metal enrichment in Svalbard, low levels of crustal dust and marine influences to southern Norway, high crustal dust and anthropogenic enrichment in the Khumbu Himalayas, and sulfur and metals attributed to quiescent degassing and volcanic activity in northern New Zealand. Rare earth element and Al/Ti elemental ratios demonstrated distinct provenance of particulates in each study region. Ca/S elemental ratio data showed seasonal denudation in Svalbard and southern Norway. Ablation season atmospheric particulate transport trajectories were mapped in each of the study regions and suggest provenance pathways. The in situ data presented provides first-order glacier surface geochemical variability as measured in the four diverse alpine glacier regions. The surface glacier geochemical data set is available from the PANGAEA database at doi:10.1594/PANGAEA.773951. This geochemical surface glacier data is relevant to glaciologic ablation rate understanding as well as satellite atmospheric and land-surface mapping techniques currently in development.

1 Introduction

A primary factor in increased glacier melt is lowered surface albedo which has been attributed to increased surface particulate coverage (Oerlemans et al., 2009). Absorbing

ESSDD
5, 107–145, 2012

particulates on snow and ice surfaces at part per million concentrations can decrease surface albedo by 5–15 % (Warren and Wiscombe, 1980), and enhance melt significantly (Paul et al., 2005; Painter et al., 2007; Yasunari et al., 2011). As alpine glacier melt and mass loss continues (Barry, 2006), understanding of surface glacier geochemical composition is an important aspect that has yet to be fully investigated.

Glacier geochemical composition is determined by geographic location, surrounding geologic and anthropogenic environment characteristics and atmospheric circulation patterns. Particulates in glaciers can indicate temperature and aridity climate conditions (Thompson, 2000; Gabrielli et al., 2010), radiative forcing alterations (Hansen and Nazarenko, 2004; Paul et al., 2005; Oerlemans et al., 2009) and particulate provenance (Kreutz and Sholkovitz, 2000; Marx et al., 2005). Specific elemental abundances (e.g. Na, Ca or Pb) can suggest natural and anthropogenic processes influencing a glacier.

Tools useful in analyzing geochemical glacier composition include atmospheric residence and transport models and satellite surface composition mapping. Atmospheric particulate residence and transport modeling can identify age of particulates as well as local and long-range circulation paths (e.g. Han and Zender, 2010; Huang et al., 2010). Satellite determination of supraglacial dust and debris geochemistry (e.g. Gleeson et al., 2010; Casey et al., 2012) allows for increased spatial and temporal glacial dust and debris analysis toward climate, radiative forcing and particulate provenance studies.

In this study, supraglacial snow, ice and debris samples were collected from four contrasting geographic, atmospheric and geologic glaciers speculated to maximize supraglacial composition diversity. Indicator elements were measured and analyzed with respect to regional geology to assess the degree of non-local impacts on glacier compositions.

ESSDD
5, 107–145, 2012

2 Background

In the atmosphere, snow and ice crystals nucleate around particulates (except when temperatures are below −38 °C and homogeneous freezing occurs) (Zimmermann et al., 2008; Cziczo et al., 2009; Knopf et al., 2011). Whether or not a particulate is at the center of a snow or ice crystal, as precipitation falls to Earth's surface, additional particulates can be assimilated. Both natural and anthropogenic particulates are transported from source areas to remote locations and incorporated in glacial geochemistry (Tatsumoto and Patterson, 1963; Barrie, 1985; Schwikowski et al., 1999; Kaspari et al., 2009).

Yet, the geochemical composition of supraglacial ice and snow evolves over days, seasons and years. Atmospheric deposition of particulates fluctuates with season, weather or emission event (e.g. a volcanic eruption, smelter emission, oceanic salts). Atmospheric wet and dry deposition, and local dust or rock fall, biotic processes, wind exposure, glacial slope and/or resurfacing of sediments from glacial flow influence supraglacial ice composition. Glacier motion can crush glacial sediments and bedrock to rock flour, allowing for remobilization of reactive trace elements within minerals to glacial ice (Tranter, 2003). Biotic processes also influence supraglacial composition (e.g. Kohshima et al., 1992; Hodson et al., 2005). For example, biota can change inorganic element oxidation states, and thus affect solubility of inorganic elements on glacier surfaces.

Glacier surface composition also evolves as chemical reactions occur. These chemical reactions are regulated by factors including solar radiation, surface temperature, wind, precipitation and the presence of melt water. In polar regions, solar radiation strongly influences seasonal atmospheric and supraglacial composition (e.g. Hg, detailed in Lu et al., 2001; Ferrari et al., 2008).

Generally, soluble species in glacier surface particulates (e.g.: Na) are washed away in runoff, or percolated downward in the snow pack with successive melt and refreeze cycles, while insoluble species are concentrated by surface sublimation

ESSDD
5, 107–145, 2012

(Colbeck, 1981; Tranter et al., 1986; Fountain, 1996; Ginot et al., 2001). The tendency for an element to be soluble is determined by intrinsic chemical properties (e.g. ionization potential, electronegativity and valency). Figure 1 displays meteoric solubility (i.e. solubility of elements in natural water with atmospheric interaction) of the elements measured in this study. This insolubility can be utilized to identify source material (Taylor and McLennan, 1985; Rudnick and Gao, 2003). Insoluble elements are targeted in this study to investigate particulate origins and anthropogenic vs. natural influences to supraglacial dust and debris. Soluble elements are used to study seasonal glacier surface abundances.

3 Geochemical influences to the study areas

The four glacier study areas located in Svalbard, southern Norway, Nepal and New Zealand contain polar and mid-latitude glaciers, Northern and Southern Hemisphere glaciers, debris covered and bare ice glaciers, as well as active volcano, marine and continental influenced glaciers. These regions provide different geographic (latitude, hemisphere, altitude), climate (precipitation, temperature, atmospheric and oceanic circulation) and glaciologic (temperate, polythermal) characteristics (Fig. 2, Table 1).

The Svalbard, Grønfjordbreen and Aldegondabreen small cirque glaciers are located on the west coast of Spitsbergen at 77.98° N, 14.12° E. This Arctic study area is influenced strongly by the North Atlantic ocean current, resulting in a relatively mild climate (mean annual temperature −6.0 °C) relative to the high northern latitude. Of the study areas, these glaciers are lowest in elevation (250–500 m), receive the least amount of precipitation (less than 400 mm per year (Hagen et al., 1993)), and are closest to the ocean as well as a local emission source. Grønfjordbreen and Aldegondabreen are less than 15 km from the ocean and coal mines.

The southern Norway (61.78° N, 7.10° E) study area consists of a mountain ice field, Jostedalsbreen, and one of its northern outlet glaciers, Bødalsbreen (elevation span from 740–1900 m). Characterized as a temperate maritime ice

ESSDD
5, 107–145, 2012

field, Jostedalsbreen experiences high precipitation year-round (approximately 1200–3000 mm) (Andreassen et al., 2005) with significant snow accumulation and annual melt due to typically warm summers (mean annual temperature 6.4 °C). Although removed from direct local emission sources, long-range transport of natural and anthropogenic particulates is a primary source of Pb, Cd, Zn and Co to southern Norway (Pacyna et al., 1984; Steinnes, 2001; Berg et al., 2008).

Of the areas studied, the Khumbu Himalaya, Nepal glaciers are closest to the Equator and highest in elevation: Ngozumpa glacier (28.00° N, 86.69° E) spans from 4700–8188 m and Khumbu glacier (27.99° N, 86.85° E) spans from 4900 m to the highest point on Earth, 8848 m. The climate in the region is strongly affected by the South Asian monsoon, mid-latitude westerlies and El Niño Southern Oscillation (ENSO) (Benn and Owen, 2002). Nepalese Khumbu Himalayan glaciers are continental "summer accumulation type" and experience summer precipitation that exceeds winter precipitation. The mean annual average temperature and precipitation in the region is −2.4 °C and 465 mm, respectively (Tartari et al., 1998; Hambrey et al., 2008). Atmospheric deposition from local continental dust is a known influence on area glaciers (e.g. Risheng et al., 2003), however, the majority of glacial debris is due to frequent rock and ice avalanches from surrounding extreme terrain (Hambrey et al., 2008). This study site has the most extensive debris cover of the areas discussed, with local geology composed primarily of quartz, feldspars, carbonates and micas (Searle et al., 2003; Casey et al., 2012).

Approximately eight small cirque glaciers lie on the upper outer flanks and in the summit craters of the active andesitic stratovolcano Mt. Ruapehu, in New Zealand (39.27° S, 175.56° E) (Dibble, 1974; Chinn, 2001). The glaciers span in elevation from 2200–2797 m and are influenced by a temperate, high precipitation, maritime climate (6.1 °C annual mean temperature, 1100 mm annual average) with seasonal snow cover. The warm acidic Crater Lake (typically between 15–40 °C) near the summit, provides a continual sulfur and to a lesser extent chloride and magnesium aerosol influence on glacier ice (Hurst et al., 1991; Werner et al., 2006). Mt. Ruapehu produces frequent

ESSDD
5, 107–145, 2012

eruptions – predominantly steam, periodically magmatic, and commonly lahars – with over 60 such documented events since 1945 (Williams, 2001; Keys, 2007; Keys and Green, 2008). The last large Mt. Ruapehu eruption occurred on 25 September 2007 (discussed in Christenson et al., 2010; Kilgour et al., 2010). From the frequent volcanic eruptions, tephra layers in glacier ice are numerous and can be up to 1/2 m thick, ranging from fine ash to ballistics, with plagioclase, pyroxene, elemental sulphur, anhydrite, pyrite, and alunite dominant mineralogy (Williams, 2001; Kilgour et al., 2010).

4 Data collection and analysis

4.1 Sample collection

Preparation for trace element supraglacial snow and ice sample collection included the following: in a clean room, soaking low density polypropylene 500 ml Nalgene bottles in an acid bath for 48 h, subsequently washing acid-soaked bottles with triple filtered deionized water, drying bottles under laminar flow, and double bagging bottles prior to transport to the field. In the field, extreme care was taken during sample collection and handling. Samples were collected with clean polyethylene gloves using standard trace element sampling procedures (e.g. Fitzgerald, 1999). While the snow and ice samples were collected in the prepped bottles, supraglacial debris samples were collected in clean polyethylene bags, obtaining approximately 100 grams of debris per sample. In total, 70 supraglacial snow, ice and debris samples were collected in accumulation and ablation seasons (except in the Khumbu Himalayas where monsoon-season sample collection was not logistically possible) as detailed in Table 1. All samples were stored at room temperature in the dark until transported for analysis to the Norwegian Institute for Water Research and the University of Oslo, Department of Geosciences in Oslo, Norway.

ESSDD
5, 107–145, 2012

4.2 Analytical methods

A Thermo Finnigan Element 2 high resolution inductively coupled plasma mass spectrometer (ICP-MS) was utilized for snow and ice major and trace element abundance measurement. All samples were nitric acid preserved (Romil brand 67–69 % HNO_3 assay for trace metal analysis, 10 %) and stored at room temperature for 2 weeks to maximize dissolution of supraglacial particulates. The following major and trace elements were measured via ICP-MS: Na, Mg, Al, Si, S, K, Ca, Ti, V, Cr, Mn, Fe, Co, Ni, Cu, Zn, As, Rb, Zr, Mo, Cd, Sn, Sb, Cs, Ba, Tl, Pb, Bi, U and rare earth elements (REE) La, Ce, Pr, Nd, Sm, Eu, Gd, Tb, Dy, Ho, Er, Tm, Yb, Lu. An internal standard spike of 10 ppb In, Ir and 50 ppb Ge, Sc, Li was utilized. External standards and blanks were run before, every tenth sample, and at the end of measurements to monitor instrument performance. Blank sample concentration values were subtracted from all sample measurement results, and three times the standard deviation of blank concentrations was utilized for the instrumental detection limit (subsequently denoted as 3σ).

Mineralogy and geochemical composition of glacier surface debris collected at the Khumbu Himalaya, Nepal and Mt. Ruapehu, New Zealand study glaciers were measured as follows. Glacial debris mineralogy was determined via powder X-ray diffraction (XRD) and geochemical composition was assessed via X-ray fluorescence spectroscopy (XRF). To prepare supraglacial debris samples for XRD and XRF analysis, debris was oven dried at 60 °C for 24 h. Debris was then crushed and ground to a fine powder of less than 125 µm particle size (via a vibratory disc mill). Powder XRD was conducted on two grams of homogenized debris sample powder via use of a Philips XPERT diffractometer (manufactured by PANalytical B.V., Almelo). Dominant mineral components were identified by semi-quantitative peak area (height × full width at half maximum) weight factor estimates (Moore, 1997) and full pattern modeling (e.g. Chipera and Bish, 2002). Ten grams of the homogenized debris sample powder were prepared into sample tablets to be measured on a Philips PW2400 XRF. The following

ESSDD
5, 107–145, 2012

oxide compounds and trace elements were measured: Na_2O, MgO, Al_2O_3, SiO_2, P_2O_5, K_2O, CaO, TiO_2, MnO, Fe_2O_3, S, V, Co, Ni, Cu, Zn, Rb, Zr, Nb, Ba, Pb, Th, and U. The accuracy of XRF results is 98 % based on calibration data.

5 Results and discussion

5.1 Element and mineral data set

Major, trace and rare earth element abundances from snow and ice samples are reported as median values from each region and sample type (Tables 2 and 3). Snow and ice major element concentrations demonstrate seasonal patterns as well as maritime, continental, and/or volcanic contributions to supraglacial dust composition at the study locations. For example, Svalbard samples displayed high amounts of characteristic sea salt aerosol deposition indicator elements, Na, S, Mg. Svalbard summer snow and ice compositions are characteristic of Arctic solute flush out (e.g. described in Pohjola et al., 2002), with depletion of Na, S, and Ca from winter to summer samples. Specifically, Grønfjordbreen winter snow samples were most enriched in Na, S, Mg and Ca, and summer Aldegondabreen ice samples were most abundant in Si, Al, Fe, Na. From the southern Norway major element glaciochemistry, Jostedalsbreen firn was highest in Fe, Al, S, Na, while Bødalsbreen ice was highest in Si, Fe, Al, Mg. Firn to ice reduced concentrations of S and Na demonstrate soluble element dissolution. The high Fe, Al, Na, Mg, and Si compositions from both southern Norway sample areas indicate the influence of local and regional dust deposition as well as slight marine influence (Pacyna and Pacyna, 2001). Khumbu Himalayan snow and ice samples from both Ngozumpa and Khumbu glaciers displayed major element compositions dominated by Ca, Fe, Si, and K, reflecting the strong continental dust influence to this region (e.g. presented in field observation and dust model results in Kang et al., 2007; Yue et al., 2009). Although monsoon season sample collection was not possible within this study, non-monsoon season surface snow concentrations are known to contain higher

ESSDD
5, 107–145, 2012

particulate loads, with soluble element peak annual concentrations (e.g. Kang et al., 2007). Mt. Ruapehu winter snow samples contained high abundance of Na, S, Mg and Ca. The S abundance in particular is likely due to the continuous aerosol emissions from the warm acidic Crater Lake as well as the frequent volcanic activity affecting the surface glacier compositions. Increased summer snow and ice abundances of Al and Ti suggest sublimation and melt flush out of soluble elements (e.g. Na).

Supraglacial debris compositions from the two debris covered glacier study regions, Khumbu Himalaya, Nepal and Mt. Ruapehu, New Zealand were distinct. The primary minerals of the Ngozumpa and Khumbu supraglacial debris were quartz, feldspars, carbonates and micas (further detailed in Casey et al., 2012). Primary minerals of the Mt. Ruapehu supraglacial debris included plagioclase and pyroxene. Median values for bulk oxide and trace elemental XRF measurements from the Khumbu Himalaya and Mt. Ruapehu, New Zealand supraglacial debris samples are presented in Table 4. The Khumbu Himalaya samples are more silica rich than the Mt. Ruapehu supraglacial debris, 63.6 % vs. 55.5 % SiO_2, respectively. The volcanically influenced Mt. Ruapehu supraglacial debris contains higher CaO, MgO and Fe_2O_3 bulk oxide and S, V, Co, Ni, Cu trace element abundance. These geochemical distinctions are as expected for continental geologic influences (e.g. SiO_2 rich) vs. volcanic influences (e.g. sulphur, metal rich).

5.2 Trace and rare Earth elemental abundances in snow and ice

Median supraglacial snow and ice trace and REE abundances are compared to geochemical standards (trace abundances to upper continental crust (UCC) composition (after McLennan, 2001) and rare earth abundances to chondrite composition (after Boynton, 1984)) to investigate geochemical variability of the distinct study regions. Due to the dilution from snow and ice, all supraglacial samples display trace and REE negative anomalies with respect to UCC and chondrite abundance (Figs. 3 and 4). The Khumbu Himalaya samples displayed highest overall trace and rare earth elemental abundances, reflecting the high dust deposition (Mahowald and others, 2009) and

ESSDD
5, 107–145, 2012

significant dust re-emission in the region, particularly during the non-monsoon season (Lee et al., 2008; Liu et al., 2011). The three other alpine glacier regions contain less debris cover and are surrounded by less arid topography and thus exhibit lower trace and rare earth elemental overall abundances. This magnitude of particulate influence at the glacier surface is quantified in Fig. 3 average magnitude abundances 1×10^{-5}–1×10^{-6} for Svalbard, Norway, and New Zealand compared with average magnitude abundances 1×10^{-3}–1×10^{-4} for Nepal (similar REE magnitude differences are displayed in Fig. 4).

Trace element to UCC abundance signatures displayed additional differences. Svalbard and southern Norway snow and ice samples revealed As, Sb and Bi enrichment, and slight enrichment in Cd, Pb, Zn, and Cu. Khumbu Himalaya snow and ice samples had relatively constant values for transition metals (Ti, V, Cr, Mn, Fe, Co, Ni) and were most enriched in As, Cs and Bi. Mt. Ruapehu snow and ice samples were least enriched in light transition metals (Ti, V) and heavy metals (Pb, U) and most enriched in As, Cd, Sb, Tl and Bi. The strong negative Zr anomalies plotted, particularly strongly in Nepal samples, are indicative of potential incomplete nitric acid digestion of the silicates (e.g. compared to HF digestion, as discussed in Osterberg et al., 2006).

Because REE are among the least soluble and geologically altered of the trace elements (Kreutz and Sholkovitz, 2000; Marx et al., 2005; Zhang et al., 2009), REE abundances can reflect supraglacial dust and debris sources. REE abundance relative to chondrite (after Boynton, 1984) is plotted in Fig. 4. Regional variations are found in both the magnitude as well as fractionation of the light (LREE: La, Ce, Pr, Nd), middle (MREE: Sm, Eu, Gd, Tb, Dy, Ho) and heavy (HREE: Er, Tm, Yb, Lu) elements. The magnitude of REE abundance was largest in the Khumbu Himalayan glacier samples, and is indicative of the high dust deposition and re-emission in the region. The three other glacier study regions, Svalbard, southern Norway, and northern New Zealand displayed a similar magnitude of REE abundance. Southern Norway snow and ice samples were enriched in LREE, with slight LREE enrichment found in Svalbard and New Zealand snow and ice samples. The Khumbu Himalayan snow and ice glacier

ESSDD
5, 107–145, 2012

samples displayed slight HREE enrichment. REE characteristics are further quantified in the elemental ratio Sect. 5.4.

5.3 Supraglacial snow, ice and debris enrichment factors relative to UCC and regional geology

Individual elemental abundances were further quantified by calculation of enrichment factors (EF) (Eq. 1). EF provide a simple, robust means to evaluate the abundance of an element in a sample relative to a reference material. Enrichment factors greater than 5 indicate significant enrichment, likely due to rock or soil dust. Enrichment factors greater than 10 indicate contribution from other natural or anthropogenic sources (Dasch and Wolff, 1989; Barbante et al., 2003) (UCC, regional loess and regional debris are used as references in this study).

$$\mathrm{EF}_x = \frac{(X/\mathrm{Ref})_{\mathrm{sample}}}{(X/\mathrm{Ref})_{\mathrm{STD}}} \quad (1)$$

Where "EF_x" corresponds to the enrichment factor of element "x", "X" is the concentration of the element to be measured, "Ref" is the concentration of the reference element (Ti in this study), "sample" indicates the concentration ratio of the sample, and "STD" indicates the concentration ratio of the standard material chosen.

Glacier surface sample EF relative to UCC, and relative to local geology are presented in Tables 5 and 6, respectively. Surface glacier snow, ice and debris enrichment of elements relative to UCC (reference element Ti) are presented for the following elements: Fe, Co, Ni, Cu, Zn, As, Mo, Cd, Sb, Rb, Ba, Pb, Bi and U. In the Svalbard supraglacial snow and ice samples, significant crustal enrichment (EF greater than 5) was found for Ni, Cu, Zn, As, Mo, Cd, Sb, Ba, Pb, Bi and U, and high (EF greater than 10) enrichment for all previous elements except Mo, Ba and U. The southern Norway snow and ice samples displayed significant crustal enrichment in Cu, Zn, As, Mo, Cd, Sb, Pb and Bi, and high enrichment of As, Cd, Sb, Pb and Bi. The Khumbu Himalaya

ESSDD
5, 107–145, 2012

snow and ice samples were significantly crustal enriched in Zn, As, Mo, Cd, Sb, Pb, Bi, and U. Greater than 10 crustal enrichment was found for As, Mo, Sb, Pb, Bi and U in Khumbu Himalaya snow and ice samples. Significant crustal enrichment was found in all Mt. Ruapehu snow and ice samples. Enrichment factors greater than 10 were measured for Co, Ni, Cu, Zn, As, Mo, Cd, Sb, Pb and Bi. From the debris samples, significant crustal enrichment of U was found in Ngozumpa debris. No significant enrichment was found for Khumbu glacier debris nor Ruapehu glacier debris.

Local geologic compositions were taken directly from Nepal and New Zealand supraglacial debris sample XRF measurements, while Spitsbergen Quaternary Loess (averaged from Advendalen samples reported in Gallet et al., 1998) was utilized for Svalbard and southern Norway EF relative to local geology calculation. Table 6 lists the EF relative to local geology calculation results from the following elements (reference element Ti): Fe, Co, Ni, Cu, Zn, Rb, Ba, Pb and U. Svalbard snow and ice displayed significant local enrichment in Ni, Cu, Zn, Ba, Pb and U, and high enrichment in Ni, Cu, Zn, and Pb. Southern Norway significant local enrichment of snow and ice samples was found for Cu, Zn and Pb, high local enrichment for Cu and Pb. Khumbu Himalaya snow and ice significant local enrichment, EF greater than 10 was found for U only. Mt. Ruapehu snow and ice significant local enrichment was found for Co, Ni, Cu, Zn, Rb, Ba, Pb and U, with high local enrichment for all listed elements except U.

The crustal vs. local enrichment calculations generally agreed well for the elements repeated in both calculations (e.g. Svalbard Pb at 43.0, 12.4 relative to crustal enrichment and 47.7, 13.7 relative to local geology). Although EF cannot be used to specify provenance nor anthropogenic vs. natural contributions (e.g. Correia et al., 2003), the EF greater than 10 values found for As, Cd, Pb and Bi suggest non-crustal and potentially anthropogenic deposition sources in the glacier study regions. In the Mt. Ruapehu study region, the strong metal crustal and local geology enrichment is likely predominantly due to the continual volcanic degassing, although a small anthropogenic contribution may be possible.

ESSDD
5, 107–145, 2012

5.4 Element abundance ratios

Elemental abundance ratios were used to demonstrate the type and degree of various geologic source contributions to supraglacial dust and debris. Three elemental abundance ratios, Ca/S, Al/Ti and Nd/Yb, are listed in Table 7 and visualized in Fig. 5.

The Ca/S ratio conveys information on relatively soluble elements Ca and S and non-quartz dominant mineral dust abundance in each of the regions. Snow to ice phase changes result in alterations to the Ca/S ratio in each of the study regions (with the exception of New Zealand where Ca and S were not measured in summer samples). Ca can be related to calcium carbonate $CaCO_3$ dust, while S is related to sulphate aerosol or volcanic influences. The Svalbard and southern Norway glacier samples exhibited high Ca and low S in ice samples, while Khumbu Himalayan snow and ice samples displayed the opposite with higher Ca in snow samples, likely due to the high amount of carbonate dust in the region. Higher S than Ca was found in Mt. Ruapehu winter snow samples, similar to the relationship found in Svalbard and southern Norway snow samples.

Both the Al/Ti and Nd/Yb elemental ratios utilize insoluble elements to provide information on the type and provenance of mineral dust in the supraglacial snow and ice samples. The Al/Ti ratio differentiates quartz type, while Nd/Yb has been utilized to pinpoint provenance (e.g. Kreutz and Sholkovitz, 2000). The particular insolubility of REE preserves geologic differences irrespective of glacial weathering and seasonal melt processes. The LREE Nd is chosen and the HREE Yb because these elements are relatively abundant and detected with greater precision than for REE potential anomaly elements. Distinct Al/Ti and Nd/Yb ranges of values can be seen from the different study area supraglacial snow and ice samples (Fig. 5). The Nd/Yb values are within the range of those reported in previous glacier snow and ice studies (e.g. Grousset et al., 1992; Ikegawa et al., 1999; Svensson et al., 2000; Kreutz and Sholkovitz, 2000; Osterberg et al., 2006). Of note, such data have not been reported in Svalbard, southern Norway or northern New Zealand.

ESSDD
5, 107–145, 2012

5.5 Surface glacier particulate influence to ablation

Because absorbing particulates on snow and ice surfaces at part per million concentrations can decrease visible surface albedo by and enhance melt significantly, total elemental particulate concentrations are briefly discussed. Single element concentrations, for example iron (Fe), ranged from 7.10 ppb in Grønfjordbreen Svalbard snow to 20.1 ppm for Ngozumpa, Khumbu Himalaya snow or sodium (Na) ranged from 19.5 ppb in Jostedalsbreen Norway snow to 2.44 ppm in Mt. Ruapehu New Zealand ice (Table 2). In order to make a simple albedo impact estimate, crude total elemental abundances were tallied and presented in the final line of Table 2. Total elemental abundance sums ranged from 0.1 ppm in Jostedalsbreen Norway snow to 96 ppm in Ngozumpa, Khumbu Himalaya snow, demonstrating that particulate loads measured in this study are likely to have albedo reducing impacts. Further, the geochemical composition of supraglacial debris, for example granitic continental vs. basaltic tephra, determines the variation of glacier surface albedo and the absorption of solar radiation. The more silica-rich debris found in Khumbu Himalaya, generally absorbs less solar radiation than the basaltic, silica-poor debris found in Mt. Ruapehu surface glacier compositions.

5.6 Modeled air mass trajectories in glacier study regions

Another means to quantify particulate transport to and deposition on glacier surfaces is use of atmospheric models. Atmospheric particulate residence times can be calculated (e.g. Han and Zender, 2010), and transport paths can be mapped (e.g. Draxler and Rolph, 2012). For this study, the HYSPLIT (HYbrid Single-Particle Lagrangian Integrated Trajectory) model (Draxler and Rolph, 2012) was utilized to estimate regional atmospheric transport patterns in each of the glacier study regions during the ablation season sample collection periods (Fig. 6). In each study region, 5-day transport paths were mapped using 24 variations in path and National Center for Environmental Prediction (NCEP) Global Data Assimilation System (GDAS) meteorologic input data. Svalbard ablation season atmospheric circulation demonstrated low-altitude Arctic air

ESSDD
5, 107–145, 2012

mass transport from the northeast. Southern Norway ablation season atmospheric transport from high-altitude Atlantic westerly movement was estimated. Khumbu Himalaya, Nepal atmospheric transport was dominated by westerlies in the November portion of the ablation season. New Zealand ablation season atmospheric particulate deposition was modeled to be transported from the west, over the Tasman Sea. The model scenarios in each region demonstrate likely ablation season transport paths, and the ability to conduct more sophisticated analysis of particulate residence times, transport paths and thus deposition to targeted glaciers.

6 Discussion

Atmospheric particulate flux and the predicted changes to particulate flux patterns have significant implications for the world's glaciers and ice sheets (Petit et al., 1999; Hansen and Nazarenko, 2004; Kaspari et al., 2009). Increased atmospheric deposition of dust, in conjunction with warming climate, could lead to greater than expected snow and ice melt rates, increased snow and ice mass loss, and ultimately contribution to sea level rise. Recent studies have also highlighted changes in spatial distribution of heavy supraglacial debris due to changing climate (Stokes et al., 2007; Scherler et al., 2011; Lambrecht et al., 2011). With warming climate, insulation provided by heavy supraglacial debris can lessen, resulting in downwasting, thinning or retreat of many glaciers (e.g. southern Himalayas, Caucasus), changes to mass flux patterns, increased meltwater discharge, and/or increased supraglacial melt and glacier lake outburst flood potential. The geochemical composition of supraglacial dust and debris influences these supraglacial energy balance variables and thus is important to study. This study adds to the understanding of supraglacial trace and rare earth elemental compositions, by providing a synoptic data set from western Svalbard, southern Norway, Khumbu Himalaya, Nepal and northern New Zealand.

In situ sampling techniques and analytical geochemical methodologies continue to evolve (e.g. immediate measurement techniques detailed in Gkinis et al., 2011).

ESSDD
5, 107–145, 2012

Currently many trace elemental measurement studies are limited by logistic constraints, which result in small sample sizes and/or inability to conduct multi-region comparisons. Small data sets also impede use of statistical methods such as cluster analysis (e.g. positive matrix factorization, principal component analysis). The most ideal description of glacial surface chemistry involves high spatial and temporal resolution data.

Satellite surface geochemical composition mapping and atmospheric dispersion and transport modeling over glacier study regions could be promising tools for investigating changing surface glacier compositions. Atmospheric modeling on multi-seasonal or annual time scales could assist in quantifying particulate deposition, at temporal scales. Satellite remote sensing techniques for describing atmospheric and surface geochemical compositions are continually improving. Satellite observations of atmospheric particulates, including mineral dust, soot, sulfide, water vapor and other components are currently mapped via spectral, lidar and thermal remote sensing techniques (e.g. Royer et al., 2010; Liu et al., 2008; Clarisse et al., 2011). Emerging research points to the ability to detect major mineral groups as well as transition metals and rare earth elements on glacier surfaces from satellite spectral remote sensing techniques (e.g. Gleeson et al., 2010; Casey et al., 2012). Yet, in situ data collection and geochemical analysis is currently the most accurate method for deriving surface glacier geochemical composition.

7 Conclusions

Trace and rare earth element supraglacial composition data are limited in published literature. This study provides an important synoptic data set of four diverse alpine glacier regions. The contrasting geographic, glaciologic, atmospheric, and geologic conditions of the regions maximize supraglacial composition diversity and allow for a first-order exploration of supraglacial geochemical composition. Surface glacier snow, ice and debris trace and rare earth element abundances and mineralogy was determined via

ESSDD
5, 107–145, 2012

ICP-MS, XRD and XRF. Measured data were compared with geochemical standards and local geology. The Khumbu Himalaya, Nepal samples contained a significantly higher magnitude of elemental abundances, including characteristic continental dust element abundances (e.g. Ca). Maritime influences of high Na content and solute flush out with Arctic spring were found in Svalbard snow and ice compositions. Volcanic influence was seen in the Mt. Ruapehu glacier sample results, with high S, Cr, Mn elemental abundances. Anthropogenic influence, was suggested by the elevated enrichment of Bi, As, Pb in all of the study regions. Rare earth element signatures were distinct in the four study areas, and suggested that more robust follow-on studies could utilize REEs to pinpoint provenance of atmospherically deposited supraglacial particulates.

XRF geochemical bulk oxide and trace element measurements offer higher accuracies and precision, free from dissolution biases. For this reason, XRF or laser ablation ICP-MS is recommended for future analytical geochemical studies. Limitations were found in use of solution ICP-MS as demonstrated by the suspected incomplete supraglacial particulate digestion of the silica-rich Khumbu Himalaya samples.

Satellite mapping of atmospheric and surface compositions are encouraged along with atmospheric particulate transport and deposition modeling. Improved quantification of glacier surface characteristics is paramount to monitoring glaciers, modeling radiative energy balance changes and estimating ice flux amidst changing climate.

Acknowledgements. This project was funded by the University of Oslo, Department of Geosciences as well as the NASA Postdoctoral Program, administered by Oak Ridge Associated Universities. R. Solberg, B. Aamaas and Ø. D. Trier are acknowledged for assistance in collecting Svalbard samples. H. Keys and H. Worsp are thanked for assistance in collecting New Zealand samples. Gratitude is extended to O. Røyset and M. Hermansen at the Norwegian Institute for Water Research for assistance with ICP-MS sample measurements. J. Olesik and P. Gabrielli at Ohio State University are acknowledged for New Zealand summer sample ICP-MS measurements. R. Xie and B. L. Berg of the University of Oslo, Department of Geosciences are thanked for assistance with XRD and XRF sample measurements. Gratitude is extended to two anonymous reviewers and D. Hall for manuscript critiques.

ESSDD
5, 107–145, 2012

References

Andreassen, L., Elvehoy, H., Kjollmoen, B., Engeset, R., and Haakensen, N.: Glacier mass-balance and length variation in Norway, Ann. Glaciol., 42, 317–325, 2005. 112

Andreassen, L. M., Paul, F., Kääb, A., and Hausberg, J. E.: Landsat-derived glacier inventory for Jotunheimen, Norway, and deduced glacier changes since the 1930s, The Cryosphere, 2, 131–145, doi:10.5194/tc-2-131-2008, 2008. 133

Barbante, C., Boutron, C., Morel, C., Ferrari, C., Jaffrezo, J., Cozzi, G., Gaspari, V., and Cescon, P.: Seasonal variations of heavy metals in central Greenland snow deposited from 1991 to 1995, J. Environ. Monitor., 5, 328–335, 2003. 118

Barrie, L.: Atmospheric particles: their physical and chemical characteristics, and deposition processes relevant to the chemical composition of glaciers, Ann. Glaciol., 7, 100–108, 1985. 110

Barry, R.: The status of research on glaciers and global glacier recession: a review, Prog. Phys. Geog., 30, 285–306, 2006. 109

Benn, D. and Owen, L.: Himalayan glacial sedimentary environments: a framework for reconstructing and dating the former extent of glaciers in high mountains, Quatern. Int., 97–98, 3–25, 2002. 112

Berg, T., Aas, W., Pacyna, J., Uggerud, H., and Vadset, M.: Atmospheric trace metal concentrations at Norwegian background sites during 25 years and its relation to European emissions, Atmos. Environ., 42, 7494–7501, 2008. 112

Boynton, W.: Developments in Geochemistry, Elsevier, Amsterdam, 63–114, 1984. 116, 117

Casey, K. A., Kääb, A., and Benn, D. I.: Geochemical characterization of supraglacial debris via in situ and optical remote sensing methods: a case study in Khumbu Himalaya, Nepal, The Cryosphere, 6, 85–100, doi:10.5194/tc-6-85-2012, 2012. 109, 112, 116, 123

Chinn, T.: Distribution of the glacal water resources of New Zealand, Journal of Hydrology (NZ), 40, 139–187, New Zealand Hydrological Society, 2001. 112

Chipera, S. and Bish, D.: FULLPAT: a full-pattern quantitative analysis program for X-ray powder diffraction using measured and calculated patterns, J. Appl. Crystallogr., 35, 744–749, 2002. 114

Christenson, B., Reyes, A., Young, R., Moebis, A., Sherburn, S., Cole-Baker, J., and Britten, K.: Cyclic processes and factors leading to phreatic eruption events: Insights from the 25 September 2007 eruption through Ruapehu Crater Lake, New Zealand, J. Volcanol. Geoth.

ESSDD
5, 107–145, 2012

Res., 191, 15–32, 2010. 113
Clarisse, L., Coheur, P., Chefdeville, S., Lacour, J., Hurtmans, D., and Clerbaux, C.: Infrared satellite observations of hydrogen sulfide in the volcanic plume of the August 2008 Kasatochi eruption, Geophys. Res. Lett., 38, L10804, doi:10.1029/2011GL047402, 2011. 123
Colbeck, S. C.: A simulation of the enrichment of atmospheric pollutants in snow cover runoff, Water Resour. Res., 17, 1383–1388, 1981. 111
Correia, A., Freydier, R., Delmas, R. J., Simões, J. C., Taupin, J.-D., Dupr, B., and Artaxo, P.: Trace elements in South America aerosol during 20th century inferred from a Nevado Illimani ice core, Eastern Bolivian Andes (6350 m asl), Atmos. Chem. Phys., 3, 1337–1352, doi:10.5194/acp-3-1337-2003, 2003. 119
Cziczo, D., Froyd, K., Gallavardin, S., Moehler, O., Benz, S., Saathoff, H., and Murphy, D.: Deactivation of ice nuclei due to atmospherically relevant surface coatings, Environ. Res. Lett., 4, 044013, doi:10.1088/1748-9326/4/4/044013, 2009. 110
Dasch, J. M. and Wolff, G.: Trace inorganic species in precipitation and their potential use in source apportionment studies, Water Air Soil Poll., 43, 401–412, 1989. 118
Dibble, R.: Volcanic seismology and accompanying activity of Ruapehu Volcano, New Zealand, Physical Volcanology, Elsevier, New York, 49–85, 1974. 112
Draxler, R. and Rolph, G.: HYSPLIT (HYbrid Single-Particle Lagrangian Integrated Trajectory) Model access via NOAA ARL READY Website (http://ready.arl.noaa.gov/HYSPLIT.php), 2012. 121
Ferrari, C., Padova, C., Fain, X., Gauchard, P.-A., Dommergue, A., Aspmo, K., Berg, T., Cairns, W., Barbante, C., Cescon, P., Kaleschke, L., Richter, A., Wittrock, F., and Boutron, C.: Atmospheric mercury depletion event study in Ny-Alesund (Svalbard) in spring 2005. Deposition and transformation of Hg in surface snow during springtime, Sci. Total Environ., 397, 167–177, 2008. 110
Fitzgerald, W.: Clean hands: Clair Patterson's crusade against environmental lead contamination, Nova Science Publ., Commack, NY, 1999. 113
Fountain, A.: Effect of snow and firn hydrology on the physical and chemical characteristics of glacial runoff, Hydrol. Process., 10, 509–521, 1996. 111
Gabrielli, P., Wegner, A., Petit, J., Delmonte, B., De Deckker, P., Gaspari, V., Fischer, H., Ruth, U., Kriews, M., Boutron, C., Cescon, P., and Barbante, C.: A major glacial-interglacial change in aeolian dust composition inferred from Rare Earth Elements in Antarctic ice, Quaternary Sci. Rev., 29, 265–273, 2010. 109

ESSDD
5, 107–145, 2012

Gallet, S., Jahn, B., Lanoë, B. V. V., Dia, A., and Rossello, E.: Loess geochemistry and its implications for particle origin and composition of the upper continental crust, Earth Planet. Sc. Lett., 156, 157–172, 1998. 119, 138

Ginot, P., Kull, C., Schwikowski, M., Schotterer, U., and Gäggeler, H.: Effects of post-depositional processes on snow composition of a subtropical glacier (Cerro Tapado, Chilean Andes), J. Geophys. Res., 106, 32375–32386, 2001. 111

Gkinis, V., Popp, T. J., Blunier, T., Bigler, M., Schüpbach, S., Kettner, E., and Johnsen, S. J.: Water isotopic ratios from a continuously melted ice core sample, Atmos. Meas. Tech., 4, 2531–2542, doi:10.5194/amt-4-2531-2011, 2011. 122

Gleeson, D., Pappalardo, R., Grasby, S., Anderson, M., Beauchamp, B., Castano, R., Chien, S., Doggett, T., Mandrake, L., and Wagstaff, K.: Characterization of a sulfur-rich Arctic spring site and field analog to Europa using hyperspectral data, Remote Sens. Environ., 114, 1297–1311, 2010. 109, 123

Grousset, F., Biscaye, P., Revel, M., Petit, J.-R., Pye, K., Joussaume, S., and Jouzel, J.: Antarctic (Dome C) ice-core dust at 18 k.y. B.P.: Isotopic constraints on origins, Earth Planet. Sc. Lett., 111, 175–182, 1992. 120

Hagen, J., Liestol, O., Roland, E., and Jorgensen, T.: Glacier Atlas of Svalbard and Jan Mayen, vol. 129, Norsk Polarinstitutt Meddelelser, 1993. 111, 133

Hambrey, M., Quincey, D., Glasser, N., Reynolds, J., Richardson, S., and Clemmens, S.: Sedimentological, geomorphological and dynamic context of debris-mantled glaciers, Mount Everest (Sagarmatha) region, Nepal, Quaternary Sci. Rev., 27, 2361–2389, 2008. 112, 133

Han, Q. and Zender, C.: Desert dust aerosol age characterized by mass-age tracking of tracers, J. Geophys. Res., 115, D22201, doi:10.1029/2010JD014155, 2010. 109, 121

Hansen, J. and Nazarenko, L.: Soot climate forcing via snow and ice albedos, P. Natl. Acad. Sci. USA, 101, 423–428, 2004. 109, 122

Hodson, A., Mumford, P., Kohler, J., and Wynn, P.: The High Arctic glacial ecosystem: new insights from nutrient budgets, Biogeochemistry, 72, 233–256, 2005. 110

Huang, L., Gong, S. L., Sharma, S., Lavoué, D., and Jia, C. Q.: A trajectory analysis of atmospheric transport of black carbon aerosols to Canadian high Arctic in winter and spring (1990–2005), Atmos. Chem. Phys., 10, 5065–5073, doi:10.5194/acp-10-5065-2010, 2010. 109

Hurst, A., Bibby, H., Scott, B., and McGuinness, M.: The heat source of Ruapehu crater lake; deductions from the energy and mass balances, J. Volcanol. Geoth. Res., 46, 1–20, 1991.

ESSDD
5, 107–145, 2012

112
Ikegawa, M., Kimura, M., Honda, K., Akabane, I., Makita, K., Motoyama, H., Fujii, Y., and Itokawa, Y.: Geographical variations of major and trace elements in East Antarctica, Atmos. Environ., 33, 1457–1467, 1999. 120
Kang, S., Zhang, Q., Kaspari, S., Qin, D., Cong, Z., Ren, J., and Mayewski, P.: Spatial and seasonal variations of elemental composition in Mt. Everest (Qomolangma) snow/firn, Atmos. Environ., 41, 7208–7218, 2007. 115, 116
Kaspari, S., Mayewski, P., Handley, M., Osterberg, E., Kang, S., Sneed, S., Hou, S., and Qin, D.: Recent increases in atmospheric concentrations of Bi, U, Cs, S and Ca from a 350-year Mount Everest ice core record, J. Geophys. Res., 114, D04302, doi:10.1029/2008JD011088, 2009. 110, 122
Keys, H.: Lahars of Ruapehu Volcano, New Zealand: risk mitigation, Ann. Glaciol., 45, 155–162, 2007. 113
Keys, H. and Green, P.: Ruapehu Lahar New Zealand 18 March 2007: Lessons for Hazard Assessment and Risk Mitigation 1995–2007, Journal of Disaster Research, 3, 284–296, 2008. 113
Kilgour, G., Manville, V., Pasqua, F. D., Graettinger, A., Hodgson, K., and Jolly, G.: The 25 September 2007 eruption of Mount Ruapehu, New Zealand: Directed ballistics, surtseyan jets, and ice-slurry lahars, J. Volcanol. Geoth. Res., 191, 1–14, 2010. 113
Knopf, D., Alpert, P., Wang, B., and Aller, J.: Stimulation of ice nucleation by marine diatoms, Nat. Geosci., 4, 88–90, 2011. 110
Kohshima, S., Seko, K., and Yoshimura, Y.: Biotic Acceleration of Glacier Melting in Yala Glacier, Langtang Region, Nepal Himalaya, in: Snow and Glacier Hydrology, vol. Proceedings of the Kathmandu Symposium, November 1992, IAHS, 309–316, 1992. 110
Kreutz, K. and Sholkovitz, E.: Major element, rare earth element, and sulfur isotopic composition of a high-elevation firn core: Sources and transport of mineral dust in central Asia, Geochem. Geophys. Geosyst., 1, 1048, doi:10.1029/2000GC000082, 2000. 109, 117, 120
Lambrecht, A., Mayer, C., Hagg, W., Popovnin, V., Rezepkin, A., Lomidze, N., and Svanadze, D.: A comparison of glacier melt on debris-covered glaciers in the northern and southern Caucasus, The Cryosphere, 5, 525–538, doi:10.5194/tc-5-525-2011, 2011. 122
Lee, K., Hur, S., Hou, S., Hong, S., Qin, X., Ren, J., Liu, Y., Rosman, K., Barbante, C., and Boutron, C.: Atmospheric pollution for trace elements in the remote high-altitude atmosphere in central Asia as recorded in snow from Mt. Qomolangma (Everest) of the Himalayas, Sci.

ESSDD
5, 107–145, 2012

Total Environ., 404, 171–181, 2008. 117
Liu, Y., Hou, S., Hong, S., Hur, S.-D., Lee, K., and Wang, Y.: Atmospheric pollution indicated by trace elements in snow from the northern slope of Cho Oyu range, Himalayas, Environ. Earth Sci., 63, 311–320, 2011. 117
Liu, Z., Liu, D., Huang, J., Vaughan, M., Uno, I., Sugimoto, N., Kittaka, C., Trepte, C., Wang, Z., Hostetler, C., and Winker, D.: Airborne dust distributions over the Tibetan Plateau and surrounding areas derived from the first year of CALIPSO lidar observations, Atmos. Chem. Phys., 8, 5045–5060, doi:10.5194/acp-8-5045-2008, 2008. 123
Lu, J., Schroeder, W., Barrie, L., Steffen, A., Welch, H., Martin, K., Lockhart, L., Hunt, R., Boila, G., and Richter, A.: Magnification of atmospheric mercury deposition to polar regions in springtime: The link to tropospheric ozone depletion chemistry, Geophys. Res. Lett., 28, 3219–3222, 2001. 110
Mahowald, N., Engelstaedter, S., Luo, C., Sealy, A., Artaxo, P., Benitez-Nelson, C., Bonnet, S., Chen, Y., Chuang, P. Y., Cohen, D. D., Dulac, F., Herut, B., Johansen, A. M., Kubilay, N., Losno, R., Maenhaut, W., Paytan, A., Prospero, J. M., Shank, L. M., and Siefert, R. L.: Atmospheric Iron Deposition: Global Distribution, Variability, and Human Perturbations, Annual Review Marine Science, 1, 245–278, 2009. 116
Marx, S., Kamber, B., and McGowan, H.: Provenance of long-travelled dust determined with ultra-trace-element composition: a pilot study with samples from New Zealand glaciers, Earth Surf. Proc. Land., 30, 699–716, 2005. 109, 117
McLennan, S.: Relationships between the trace element composition of sedimentary rocks and upper continental crust, Geochem. Geophys. Geosyst., 2, 24 pp., doi:10.1029/2000GC000109, 2001. 116
Moore, D. M. and Reynolds, C.: X-ray diffraction and the identification and analysis of clay minerals, Oxford University Press, New York, 2nd edn., 1997. 114
Oerlemans, J., Giesen, R., and van den Broeke, M.: Retreating alpine glaciers: increased melt rates due to accumulation of dust (Vadret da Morteratsch, Switzerland), J. Glaciol., 55, 729–736, 2009. 108, 109
Osterberg, E., Handley, M., Sneed, S., Mayewski, P., and Kreutz, K.: Continuous Ice Core Melter System with Discrete Sampling for Major Ion, Trace Element, and Stable Isotope Analyses, Environ. Sci. Technol., 40, 3355–3361, 2006. 117, 120
Pacyna, J. and Pacyna, E.: An assessment of global and regional emissions of trace metals to the atmosphere from anthropogenic sources worldwide, Environ. Rev., 9, 269–298, 2001.

ESSDD
5, 107–145, 2012

115
Pacyna, J., Semb, A., and Hanssen, J.: Emission and long-range transport of trace elements in Europe, Tellus B, 36B, 163–178, 1984. 112
Painter, T., Barrett, A., Landry, C., Neff, J., Cassidy, M., Lawrence, C., McBride, K., and Farmer, G.: Impact of disturbed desert soils on duration of mountain snow cover, Geophys. Res. Lett., 34, L12502, doi:10.1029/2007GL030284, 2007. 109
Paul, F., Machguth, H., and Kääb, A.: On the impact of glacier albedo under conditions of extreme glacier melt: the summer of 2003 in the Alps, in: EARSeL eProceedings, vol. 4, 2005. 109
Petit, J., Jouzel, J., Raynaud, D., Barkov, N., Barnola, J.-M., Basile, I., Benders, M., Chappellaz, J., Davis, M., Delaygue, G., Delmotte, M., Kotlyakov, V., Legrand, M., Lipenkov, V., Lorius, C., Pèpin, L., Ritz, C., Saltzman, E., and Stievenard, M.: Climate and atmospheric history of the past 420,000 years from the Vostok ice core, Antarctica, Nature, 399, 429–436, 1999. 122
Pohjola, V. A., Moore, J. C., Isaksson, E., Jauhiainen, T., van de Wal, R. S. W., Martma, T., Meijer, H. A. J., and Vaikmäe, R.: Effect of periodic melting on geochemical and isotopic signals in an ice core from Lomonosovfonna, Svalbard, J. Geophys. Res., 107, 4036, doi:10.1029/2000JD000149, 2002. 115
Risheng, L., Jun, C., Gengnian, L., and Zhijiu, C.: Characteristics of the subglacially-formed debris-rich chemical deposits and related subglacial processes of Qiangyong Glacier, Tibet, J. Geogr. Sci., 13, 455–462, 2003. 112
Royer, P., Raut, J.-C., Ajello, G., Berthier, S., and Chazette, P.: Synergy between CALIOP and MODIS instruments for aerosol monitoring: application to the Po Valley, Atmos. Meas. Tech., 3, 893–907, doi:10.5194/amt-3-893-2010, 2010. 123
Rudnick, R. and Gao, S.: Composition of the Continental Crust, in: Treatise on Geochemistry, edited by: Holland, H. D. and Turekian, K. K., Pergamon, Oxford, 1–64, 2003. 111, 140
Scherler, D., Bookhagen, B., and Strecker, M.: Spatially variable response of Himalayan glaciers to climate change affected by debris cover, Nat. Geosci., 4, 156–159, 2011. 122
Schwikowski, M., Döscher, A., Gäggler, H., and Schotterer, U.: Anthropogenic versus natural sources of atmospheric sulphate from an Alpine ice core, Tellus B, 51, 938–951, 1999. 110
Searle, M., Simpson, R., Law, R., Parrish, R., and Waters, D.: The structural geometry, metamorphic and magmatic evolution of the Everest massif, High Himalaya of Nepal-South Tibet, J. Geol. Soc. London, 160, 345–366, 2003. 112

ESSDD
5, 107–145, 2012

Steinnes, E.: Metal Contamination of the Natural Environment in Norway from Long Range Atmospheric Transport, Water Air Soil Poll., 1, 449–460, 2001. 112
Stokes, C., Popovnin, V., Aleynikov, A., Gurney, S., and Shahgedanova, M.: Recent glacier retreat in the Caucasus Mountains, Russia and associated increase in supraglacial debris cover and supra-, proglacial lake development, Ann. Glaciol., 46, 195–203, 2007. 122
Svensson, A., Biscaye, P., and Grousset, F.: Characterization of late glacial continental dust in the Greenland Ice Core Project ice core, J. Geophys. Res., 105, 4637–4656, 2000. 120
Tartari, G., Verza, G., and Bertolami, L.: Meteorological data at the Pyramid Observatory Laboratory (Khumbu Valley, Sagarmatha National Park, Nepal), Limnology of high altitude lakes in the Mt. Everest Region, Nepal, 57, 23–40, 1998. 112, 133
Tatsumoto, M. and Patterson, C.: Concentrations of common lead in some Atlantic and Mediterranean waters and in snow, Nature, 199, 350–352, 1963. 110
Taylor, S. and McLennan, S.: The Continental Crust: its Composition and Evolution, Blackwell Scientific, Palo Alto, CA, 1985. 111, 140
Thompson, L.: Ice core evidence for climate change in the Tropics: implications for our future, Quaternary Sci. Rev., 19, 19–35, 2000. 109
Tranter, M.: Geochemical Weathering in Glacial and Proglacial Environments, in: Treatise on Geochemistry, edited by: Holland, H. D. and Turekian, K. K., Pergamon, Oxford, 189–205, 2003. 110
Tranter, M., Brimblecombe, P., Davies, T., Vincent, C., Abrahams, P., and Blackwood, I.: The composition of snowfall, snowpack and meltwater in the Scottish Highlands – evidence for preferential elution, Atmos. Environ., 20, 517–525, 1986. 111
Warren, S. and Wiscombe, W.: A Model for the Spectral Albedo of Snow. II: Snow Containing Atmospheric Aerosols, J. Atmos. Sci., 37, 2734–2745, 1980. 109
Werner, C., Christenson, B., Hagerty, M., and Britten, K.: Variability of volcanic gas emissions during a crater lake heating cycle at Ruapehu Volcano, New Zealand, J. Volcanol. Geoth. Res., 154, 291–302, 2006. 112
Williams, K.: Volcanoes of the South Wind, Tongariro Natural History, P.O. Box 238, Turangi, ISBN: 0-473-07537-7, 2001. 113
Yasunari, T., Koster, R., Lau, K.-M., Aoki, T., Sud, Y., Yamazaki, T., Motoyoshi, H., and Kodama, Y.: Influence of dust and black carbon on the snow albedo in the NASA Goddard Earth Observing System version 5 land surface model, J. Geophys. Res., 116, D02210, doi:10.1029/2010JD014861, 2011. 109

ESSDD
5, 107–145, 2012

Yue, X., Wang, H., Wang, Z., and Fan, K.: Simulation of dust aerosol radiative feedback using the Global Transport Model of Dust: 1. Dust cycle and validation, J. Geophys. Res., 114, D10202, doi:10.1029/2008JD010995, 2009. 115

Zhang, Q., Kang, S., Kaspari, S., Li, C., Qin, D., Mayewski, P., and Hou, S.: Rare earth elements in an ice core from Mt. Everest: Seasonal variations and potential sources, Atmos. Res., 94, 300–312, 2009. 117

Zimmermann, F., Weinbruch, S., Schutz, L., Hofmann, H., Ebert, M., Kandler, K., and Worringen, A.: Ice nucleation properties of the most abundant mineral dust phases, J. Geophys. Res., 113, D23204, doi:10.1029/2008JD010655, 2008. 110

ESSDD

5, 107–145, 2012

Table 1. Characteristics of glacier study regions.

Study region, glacier (latitude, longitude)	Glacier type, influences	Mean annual temp., precip. data, elevation (m a.s.l.)	Dates glacier surface samples collected	Number of glacier surface samples, (ID)
Svalbard, Grønfjordbreen Aldegondabreen (77.98° N, 14.12° E)	Arctic, small valley, polythermal. maritime influences	−6.0 °C, >400 mm[a] 250–500 m[b]	17, 18 April 2009 18 July 2009	8 snow (1a) 2 ice (1b)
Norway, Jostedalsbreen Bødalsbreen (61.78° N, 7.10° E)	Ice field and outlet valley glacier, temperate slight maritime influence	6.4 °C, 1200–3000 mm[c] 740–1990 m[d]	24–27 June 2009	3 snow (2a) 4 ice (2b)
Nepal, Ngozumpa Khumbu (28.00° N, 86.69° E)	Debris covered continental valley glaciers. Temperate, summer accumulation	−2.4 °C, 465 mm[e] 4900–8848 m[f]	26–27 November 2009 4–6 December 2009	6 snow (3a), 4 ice (3b), 8 debris (3c) 2 snow (3d), 6 ice (3e), 14 debris (3f)
New Zealand, Mt. Ruapehu[g] (39.27° S, 175.56° E)	Cirque glaciers volcanic influences	6.1 °C, 1100 mm[h] 2200–2797 m[i]	28 August 2009 5 March 2010	9 snow (4a) 1 snow (4b), 1 ice (4c), 2 debris (4d)

[a] Svalbard coastal region mean annual temperature and precipitation from Hagen et al. (1993).
[b] Norwegian Polar Institute (2004).
[c] Norwegian Meteorological Institute (1961–1990).
[d] Andreassen et al. (2008).
[e] From Tartari et al. (1998) as measured at Pyramid Meteorological Station (5050 m a.s.l.) from 1990–1996 though agree well with previous studies from the 1970s and 1992. Note 87 % of precipitation was found to occur solely in monsoon season (June–September).
[f] Hambrey et al. (2008).
[g] Mt. Ruapehu winter snow samples were collected from Whakapapa, Paretaetaitonga and Whangaehu glaciers, and summer snow, ice and debris samples were collected from Mangatoetoenui glacier.
[h] New Zealand National Institute of Water and Atmospheric Research records, accessed 2010 for Whakapapa Village, elevation 1100 m.
[i] New Zealand Department of Conservation (2004).

ESSDD
5, 107–145, 2012

Table 2. Median major and trace elemental abundances (ppb) for snow and ice samples by region. Values below instrumental limit of detection (LOD, 3σ) are given in parentheses or indicated by "<dl" if measured at zero.

Element	LOD	Svalbard		Norway		Nepal				New Zealand		
	(3σ)	1a ($n=8$)	1b ($n=2$)	2a ($n=3$)	2b ($n=4$)	3a ($n=6$)	3b ($n=4$)	3d ($n=2$)	3e ($n=6$)	4a ($n=9$)	4b ($n=1$)	4c* ($n=1$)
Na	10.6	1.44×10^{3}	619	19.5	219	653	201	381	76.4	747	128	2.44×10^{3}
Mg	1.61	172	177	10.8	979	8.59×10^{3}	205	5.75×10^{3}	584	102	–	–
Al	2.16	15.3	833	24.4	1.96×10^{3}	2.02×10^{4}	337	1.07×10^{4}	1.03×10^{3}	18.6	194	1.05×10^{4}
Si	53.8	<dl	1.23×10^{3}	(7.69)	3.37×10^{3}	1.29×10^{4}	1.24×10^{3}	1.44×10^{4}	1.66×10^{3}	<dl	–	–
S	29.5	194	92.3	(19.0)	135	112	454	325	134	136	–	–
K	9.93	55.9	221	(7.78)	697	1.18×10^{4}	739	5.82×10^{3}	787	37.2	–	–
Ca	3.64	76.5	199	4.97	758	1.68×10^{4}	1.03×10^{4}	3.03×10^{4}	2.64×10^{3}	52.5	–	–
Ti	6.21×10^{-2}	0.597	47.1	2.41	209	3.70×10^{3}	44.3	1.58×10^{3}	168	0.299	1.25	32.4
V	3.10×10^{-2}	3.97×10^{-2}	3.40	3.48×10^{-2}	6.67	70.0	1.22	32.0	3.19	3.58×10^{-2}	5.30×10^{-2}	1.11
Cr	1.88×10^{-2}	3.49×10^{-2}	1.17	2.92×10^{-2}	4.32	55.9	0.691	29.8	2.98	0.108	5.39×10^{-2}	1.75
Mn	1.88×10^{-2}	0.166	6.33	0.524	42.9	489	6.93	425	30.8	0.809	1.83	25.4
Fe	1.22	7.10	757	25.5	2.89×10^{3}	2.01×10^{4}	374	1.86×10^{4}	1.70×10^{3}	18.6	26.5	351
Co	1.81×10^{-3}	5.60×10^{-3}	0.37	1.75×10^{-2}	1.29	16.9	0.273	10.9	0.969	2.63×10^{-2}	0.166	2.61
Ni	5.79×10^{-2}	8.50×10^{-2}	0.83	<dl	3.93	29.8	0.364	22.3	1.90	8.18×10^{-2}	–	–
Cu	4.27×10^{-2}	8.08×10^{-2}	1.19	0.125	7.39	34.7	1.09	21.2	1.67	8.06×10^{-2}	0.278	13.5
Zn	0.217	0.871	1.61	(7.41×10^{-2})	18.9	86.6	4.90	60.5	5.43	10.1	0.565	4.74
As	2.28×10^{-2}	(9.28×10^{-3})	0.80	<dl	2.26	12.7	6.56	8.18	0.559	<dl	0.300	0.667
Rb	9.30×10^{-3}	4.97×10^{-2}	1.96	9.18×10^{-2}	6.43	254	5.49	99.9	12.6	6.51×10^{-2}	0.205	2.21
Zr	1.04×10^{-2}	3.47×10^{-2}	2.20	2.90×10^{-2}	0.583	0.287	2.10×10^{-2}	0.133	3.42×10^{-2}	4.66×10^{-2}	–	–
Mo	5.03×10^{-3}	(6.66×10^{-4})	0.133	(8.69×10^{-4})	0.265	0.191	0.480	0.162	1.76×10^{-2}	1.74×10^{-2}	6.59×10^{-3}	1.62×10^{-2}
Cd	3.87×10^{-2}	(4.93×10^{-3})	(2.43×10^{-2})	(2.10×10^{-3})	5.73×10^{-2}	0.195	(5.91×10^{-3})	0.114	(1.01×10^{-2})	(4.45×10^{-3})	(5.83×10^{-3})	(3.32×10^{-2})
Sn	9.37×10^{-3}	1.41×10^{-2}	0.241	2.10×10^{-2}	3.02	9.09	0.242	2.12	0.309	<dl	(2.68×10^{-3})	6.21×10^{-2}
Sb	3.40×10^{-3}	9.15×10^{-3}	0.138	1.65×10^{-2}	0.776	6.89×10^{-2}	4.86×10^{-2}	0.126	(2.99×10^{-3})	(2.04×10^{-3})	8.42×10^{-3}	2.33×10^{-2}
Cs	2.06×10^{-3}	(6.79×10^{-4})	0.203	4.09×10^{-3}	0.425	62.7	1.14	30.2	3.07	(1.01×10^{-3})	–	–
Ba	4.44×10^{-2}	0.713	19.9	0.308	14.9	185	3.24	96.3	11.5	0.398	–	–
Tl	1.60×10^{-4}	2.15×10^{-4}	3.40×10^{-2}	<dl	6.53×10^{-2}	1.48	2.05×10^{-2}	0.514	6.37×10^{-2}	<dl	1.59×10^{-2}	0.304
Pb	1.66×10^{-3}	0.106	2.42	0.193	56.1	26.6	0.708	67.8	1.65	4.53×10^{-2}	1.56×10^{-2}	0.316
Bi	1.60×10^{-4}	2.60×10^{-3}	6.59×10^{-2}	6.11×10^{-3}	1.28	8.39	0.179	4.76	0.342	4.82×10^{-3}	2.60×10^{-3}	5.65×10^{-2}
U	5.30×10^{-4}	3.30×10^{-3}	0.161	2.69×10^{-3}	0.276	9.43	21.1	10.3	1.21	1.38×10^{-3}	4.63×10^{-3}	2.28×10^{-2}
Σ (ppm)		2.0	4.2	0.12	11	96	14	89	8.9	1.1	0.35	13

* Where the following notations represent the following samples: 1a Grønfjordbreen snow, 1b Aldegondabreen ice, 2a Jostedalsbreen snow, 2b Bødalsbreen ice, 3a Ngozumpa snow, 3b Ngozumpa ice, 3d Khumbu snow, 3e Khumbu ice, 4a Ruapehu winter snow, 4b Ruapehu summer snow, and 4c Ruapehu summer ice.

ESSDD
5, 107–145, 2012

Table 3. Median rare earth elemental abundances (ppt) for snow and ice samples by region. Values below instrumental limit of detection (LOD, 3σ) are given in parentheses or indicated by "<dl" if measured at zero.

Element	LOD	Svalbard		Norway		Nepal				New Zealand		
	(3σ)	1a ($n=8$)	1b ($n=2$)	2a ($n=3$)	2b ($n=4$)	3a ($n=6$)	3b ($n=4$)	3d ($n=2$)	3e ($n=6$)	4a ($n=9$)	4b ($n=1$)	4c* ($n=1$)
La	0.47	12.2	1.03×10^{3}	57.9	9.59×10^{3}	8.32×10^{3}	107	8.94×10^{3}	719	23.1	71.8	600
Ce	1.01	53.0	2.16×10^{3}	110	1.82×10^{4}	1.92×10^{4}	251	1.93×10^{4}	1.49×10^{3}	85.1	217	1.73×10^{3}
Pr	0.28	3.85	281	10.3	2.16×10^{3}	2.64×10^{3}	28.1	2.51×10^{3}	186	7.58	23.9	199
Nd	1.46	15.5	1.15×10^{3}	33.2	7.85×10^{3}	1.22×10^{4}	120	1.07×10^{4}	749	29.2	94.9	804
Sm	1.37	3.32	248	6.17	1.24×10^{3}	3.85×10^{3}	35.2	3.10×10^{3}	198	6.49	19.5	195
Eu	0.52	<dl	50.2	<dl	166	694	5.22	564	32.4	0.561	4.26	53.9
Gd	0.67	3.48	234	7.33	1.21×10^{3}	4.75×10^{3}	38.5	3.92×10^{3}	225	6.04	18.4	186
Tb	0.35	(0.102)	24.2	(0.331)	94.4	785	5.04	628	31.7	0.482	2.25	25.9
Dy	0.34	1.33	155	3.74	530	5.39×10^{3}	34.1	4.06×10^{3}	227	2.63	11.2	147
Ho	0.27	(0.200)	28.8	0.556	101	913	7.20	736	37.7	0.387	2.11	27.8
Er	0.26	0.786	73.9	1.50	286	2.42×10^{3}	15.1	2.01×10^{3}	102	2.42	5.74	76.0
Tm	0.45	(8.86×10^{-2})	10.4	(0.348)	33.4	316	2.21	291	15.3	(0.352)	0.879	10.5
Yb	0.30	0.732	59.8	(0.151)	212	1.87×10^{3}	12.2	1.69×10^{3}	87.9	1.29	5.74	67.3
Lu	0.22	<dl	8.67	(2.20×10^{-2})	32.0	242	1.65	220	11.4	<dl	0.938	9.66
ΣREE	–	94.2	5.52×10^{3}	232	4.17×10^{4}	6.36×10^{4}	663	5.87×10^{4}	4.11×10^{3}	165	479	4.14×10^{3}

* Where the following notations represent the following samples: 1a Grønfjordbreen snow, 1b Aldegondabreen ice, 2a Jostedalsbreen snow, 2b Bødalsbreen ice, 3a Ngozumpa snow, 3b Ngozumpa ice, 3d Khumbu snow, 3e Khumbu ice, 4a Ruapehu winter snow, 4b Ruapehu summer snow, and 4c Ruapehu summer ice.

ESSDD
5, 107–145, 2012

Table 4. Khumbu Himalaya, Nepal and Ruapehu, New Zealand glacier debris median bulk oxide weight percents and trace element abundances (ppm) as determined by XRF.

Region	Na_2O	MgO	Al_2O_3	SiO_2	P_2O_5	K_2O	CaO	TiO_2	MnO	Fe_2O_3
Nepal										
Ngozumpa glacier debris, 3c ($n = 8$)	2.93	1.49	13.7	63.9	0.140	3.95	2.32	0.500	7.00×10^{-2}	4.00
Khumbu glacier debris, 3f ($n = 14$)	2.33	2.21	14.0	63.3	0.125	3.96	2.58	0.710	7.00×10^{-2}	5.37
New Zealand										
Mangatoetoenui glacier debris, 4d ($n = 2$)	2.89	4.23	15.0	55.5	8.00×10^{-2}	1.24	7.07	0.665	0.120	7.69

Region	S	V	Co	Ni	Cu	Zn	Rb	Zr	Nb	Ba	Pb	Th	U
Nepal													
Ngozumpa glacier debris, 3c ($n = 8$)	12.5	45.5	11.5	26.5	17.0	76.5	313	181	17.5	407	41.0	18.5	10.5
Khumbu glacier debris, 3f ($n = 14$)	201	71.5	15.0	34.5	22.0	89.5	244	214	19.0	568	37.0	20.0	8.50
New Zealand													
Mangatoetoenui glacier debris, 4d ($n = 2$)	1.81×10^3	196	27.5	60.5	49.5	66.0	51.0	112	5.50	274	10.5	5.00	2.50

ESSDD
5, 107–145, 2012

Table 5. Snow, ice and debris enrichment of elements relative to UCC (reference element Ti) are listed. EF values with significant enrichment (i.e. EF > 5) are displayed in **bold**. Elements with sample measurements below instrumental detection limits or not measured (3c, 3f, 4b, 4c) are indicated by "–".

EF relative to UCC	Svalbard		Norway		Nepal					New Zealand				
	1a ($n=8$)	1b ($n=2$)	2a ($n=3$)	2b ($n=4$)	3a ($n=6$)	3b ($n=4$)	3c ($n=8$)	3d ($n=2$)	3e ($n=6$)	3f ($n=14$)	4a ($n=9$)	4b ($n=1$)	4c ($n=1$)	4d* ($n=2$)
Fe	1.39	1.88	1.24	1.62	0.638	0.988	1.09	1.38	1.18	1.03	**7.30**	2.47	1.27	1.58
Co	2.26	1.91	1.75	1.49	1.11	1.49	0.926	1.66	1.39	0.850	**21.2**	**32.1**	**19.4**	1.66
Ni	**13.3**	1.65	–	1.75	0.752	0.764	0.824	1.31	1.05	0.755	**25.5**	–	–	1.41
Cu	**22.2**	4.14	**8.53**	**5.79**	1.54	4.04	0.930	2.19	1.63	0.848	**44.2**	**36.5**	**68.3**	2.04
Zn	**84.4**	1.98	1.77	**5.22**	1.35	**6.38**	1.47	2.21	1.86	1.21	**1950**	**26.1**	**8.45**	0.956
As	**44.0**	**46.7**	–	**29.6**	**9.40**	**404**	–	14.1	**9.07**	–	–	**654**	**56.3**	–
Mo	3.05	**7.70**	0.985	**3.47**	0.141	**29.6**	–	0.280	0.286	–	**159**	**14.4**	1.36	–
Cd	**346**	**21.5**	**36.5**	**11.5**	2.20	**5.58**	–	3.01	2.51	–	**622**	**195**	**42.8**	–
Sb	**314**	**59.9**	**141**	**76.1**	0.382	**22.5**	–	1.63	0.364	–	**140**	**138**	**14.7**	–
Rb	3.05	1.53	1.39	1.12	2.52	4.54	3.82	2.31	2.73	2.10	**7.97**	**6.01**	2.50	0.468
Ba	**8.91**	3.16	0.952	0.532	0.373	0.545	1.01	0.453	0.509	0.995	**9.91**	–	–	0.512
Pb	**43.0**	**12.4**	**19.3**	**64.7**	1.74	3.85	3.30	**10.3**	2.36	2.10	**36.5**	3.00	2.35	0.635
Bi	**141**	**45.2**	**81.8**	**197**	**73.3**	**131**	–	**97.2**	**65.5**	–	**520**	**67.1**	**56.2**	–
U	**8.09**	**5.01**	1.64	1.93	3.74	**696**	**5.13**	**9.54**	**10.5**	2.92	**6.78**	**5.42**	1.03	0.918

* Where the following notations represent the following samples: 1a Grønfjordbreen snow, 1b Aldegondabreen ice, 2a Jostedalsbreen snow, 2b Bødalsbreen ice, 3a Ngozumpa snow, 3b Ngozumpa ice, 3c Ngozumpa debris, 3d Khumbu snow, 3e Khumbu ice, 3f Khumbu debris, 4a Ruapehu winter snow, 4b Ruapehu summer snow, 4c Ruapehu summer ice and 4d Ruapehu debris.

ESSDD
5, 107–145, 2012

Table 6. Elemental enrichment of Svalbard and southern Norway snow and ice samples relative to Spitsbergen loess (reference element Ti) (from Adventdalen samples reported in Gallet et al., 1998). Nepal and New Zealand snow and ice sample elemental enrichments are presented relative to XRF measured supraglacial debris measurements conducted in this study (as reported in Table 4). EF values with significant enrichment (i.e. EF > 5) are displayed in **bold**. Elements with sample measurements below instrumental detection limits or not measured (4b, 4c) are indicated by "–".

EF relative to local geology	Svalbard		Norway		Nepal				New Zealand		
	1a ($n = 8$)	1b ($n = 2$)	2a ($n = 3$)	2b ($n = 4$)	3a ($n = 6$)	3b ($n = 4$)	3d ($n = 2$)	3e ($n = 6$)	4a ($n = 9$)	4b ($n = 1$)	4c* ($n = 1$)
Fe	1.58	2.13	1.40	1.83	0.583	0.904	1.33	1.14	4.62	1.57	0.802
Co	2.60	2.20	2.01	1.71	1.19	1.61	1.95	1.63	**12.7**	**19.3**	**11.7**
Ni	**22.3**	2.76	–	2.94	0.913	0.928	1.74	1.39	**18.0**	–	–
Cu	**35.3**	**6.57**	**13.5**	**9.20**	1.65	4.34	2.59	1.92	**21.7**	**17.9**	**33.5**
Zn	**85.3**	2.07	1.86	**5.47**	0.918	4.33	1.82	1.53	**2040**	**27.3**	**8.84**
Rb	4.72	2.37	2.16	1.74	0.658	1.19	1.10	1.30	**17.0**	**12.8**	**5.34**
Ba	**8.37**	2.97	0.895	0.500	0.368	0.539	0.456	0.512	**19.3**	–	–
Pb	**47.7**	**13.7**	**21.4**	**71.7**	0.526	1.17	4.93	1.13	**57.5**	4.72	3.70
U	**9.42**	5.84	1.90	2.25	0.729	**136**	3.26	3.61	**7.38**	**5.90**	1.12

* Where the following notations represent the following samples: 1a Grønfjordbreen snow, 1b Aldegondabreen ice, 2a Jostedalsbreen snow, 2b Bødalsbreen ice, 3a Ngozumpa snow, 3b Ngozumpa ice, 3d Khumbu snow, 3e Khumbu ice, 4a Ruapehu winter snow, 4b Ruapehu summer snow and 4c Ruapehu summer ice.

ESSDD
5, 107–145, 2012

Table 7. Elemental ratios for snow, ice and debris samples from each study region.

Element	Svalbard		Norway		Nepal						New Zealand			
	1a ($n = 8$)	1b ($n = 2$)	2a ($n = 3$)	2b ($n = 4$)	3a ($n = 6$)	3b ($n = 4$)	3c ($n = 8$)	3d ($n = 2$)	3e ($n = 6$)	3f ($n = 14$)	4a ($n = 9$)	4b ($n = 1$)	4c ($n = 1$)	4d* ($n = 2$)
Ca/S	0.394	2.16	0.262	5.62	150	22.7	1.33×10^3	93.2	19.8	91.7	0.387	–	–	27.9
Al/Ti	25.6	17.7	10.1	9.36	5.46	7.59	24.2	6.76	6.13	17.4	62.2	155	324	19.9
Nd/Yb	21.2	19.2	<dl	37.1	6.54	9.84	–	6.35	8.52	–	22.7	16.5	12.0	–

* Where the following notations represent the following samples: 1a Grønfjordbreen snow, 1b Aldegondabreen ice, 2a Jostedalsbreen snow, 2b Bødalsbreen ice, 3a Ngozumpa snow, 3b Ngozumpa ice, 3c Ngozumpa debris, 3d Khumbu snow, 3e Khumbu ice, 3f Khumbu debris, 4a Ruapehu winter snow, 4b Ruapehu summer snow, 4c Ruapehu summer ice, and 4d Ruapehu debris.

ESSDD
5, 107–145, 2012

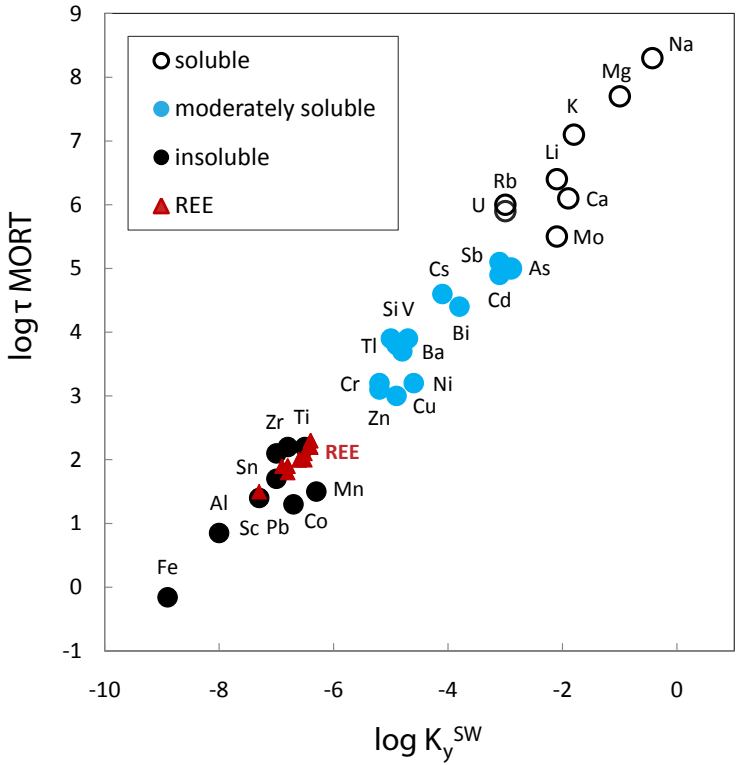

Fig. 1. The plot presents the meteoric solubility (i.e. solubility of elements in natural water with atmospheric interaction) of the elements measured in the study regions, where the geochemical reference standard Mean Ocean Residence Time (MORT) is given relative to the chemical partition coefficient (of sea water to upper continental crust) (chemical data after Taylor and McLennan, 1985; Rudnick and Gao, 2003).

ESSDD
5, 107–145, 2012

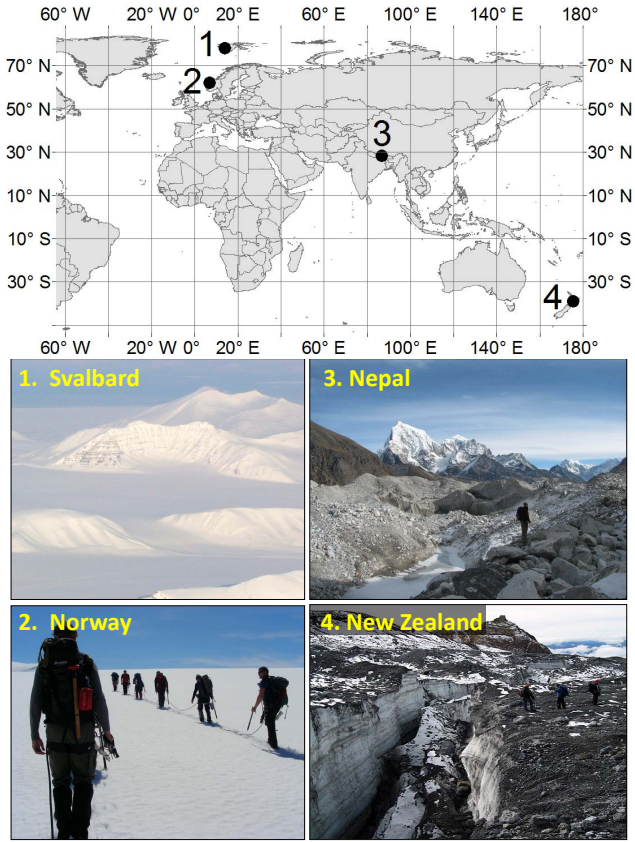

Fig. 2. (Upper) Map depicting study glaciers Grønfjordbreen and Aldegondabreen in western Svalbard (1), Bødalsbreen outlet glacier and parent Jostedalsbreen ice field in southern Norway (2), Ngozumpa and Khumbu glaciers in Khumbu Himalaya, Nepal (3) and Mt. Ruapheu, New Zealand glaciers (4). (Lower) Field photos of study regions as labeled. Note, the Svalbard picture was taken by R. Solberg, and the New Zealand picture was taken by M. Hambrey.

ESSDD
5, 107–145, 2012

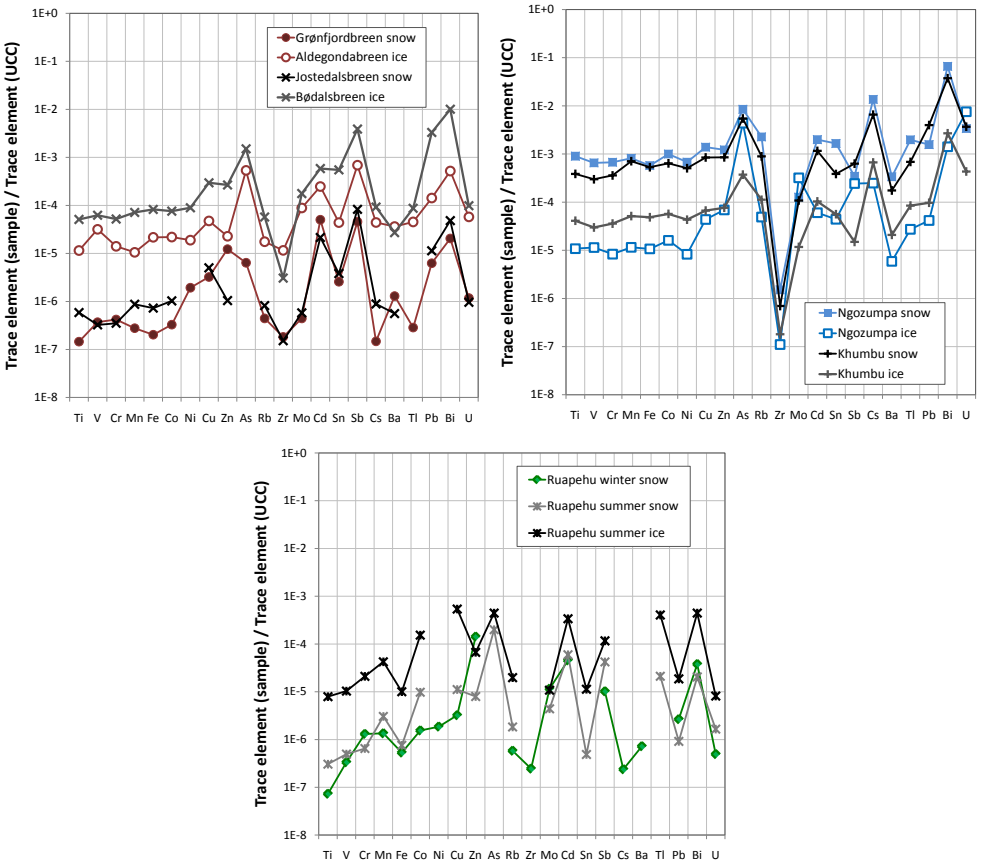

Fig. 3. Log scale trace element to upper continental crust snow and ice signatures for each of the study regions. Svalbard and southern Norway snow and ice elemental abundances are displayed in the top chart, followed by the Khumbu Himalaya, Nepal abundances in the middle chart, and Mt. Ruapehu New Zealand abundances displayed in the lower chart.

ESSDD
5, 107–145, 2012

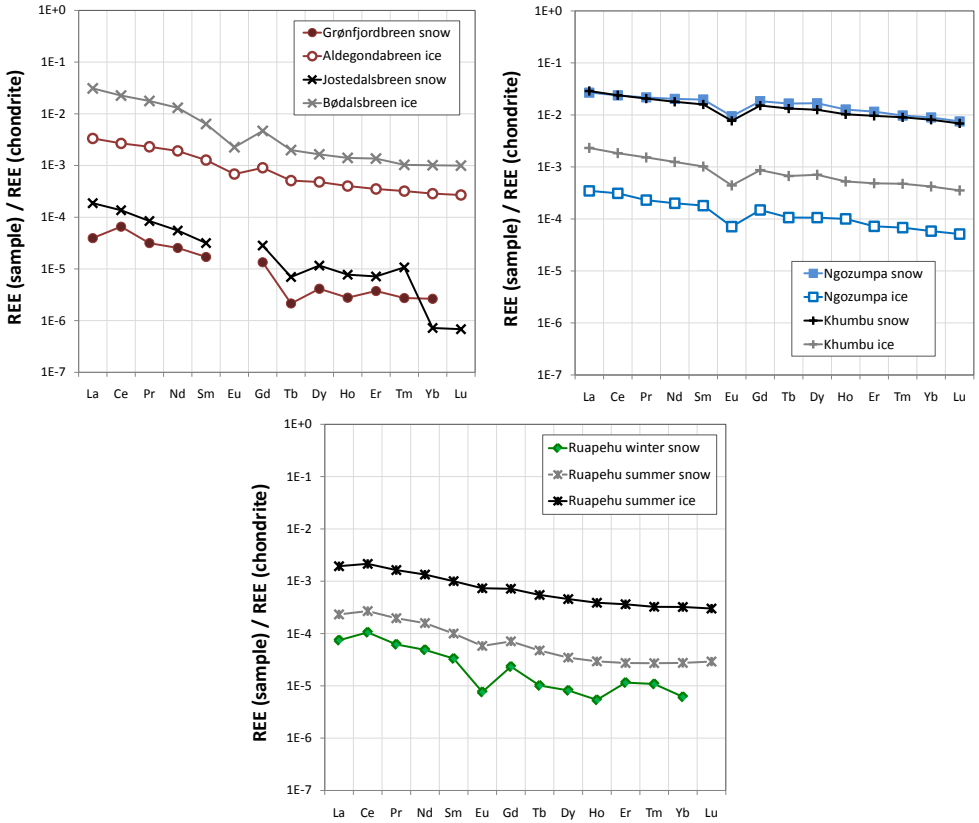

Fig. 4. Log scale REE element relative to chondrite snow and ice signatures for each of the study regions. Svalbard and southern Norway snow and ice REE abundances are shown in the top chart, followed by the Khumbu Himalaya, Nepal REE abundances in the middle chart, and Mt. Ruapehu, New Zealand REE abundances displayed in the lower chart.

ESSDD
5, 107–145, 2012

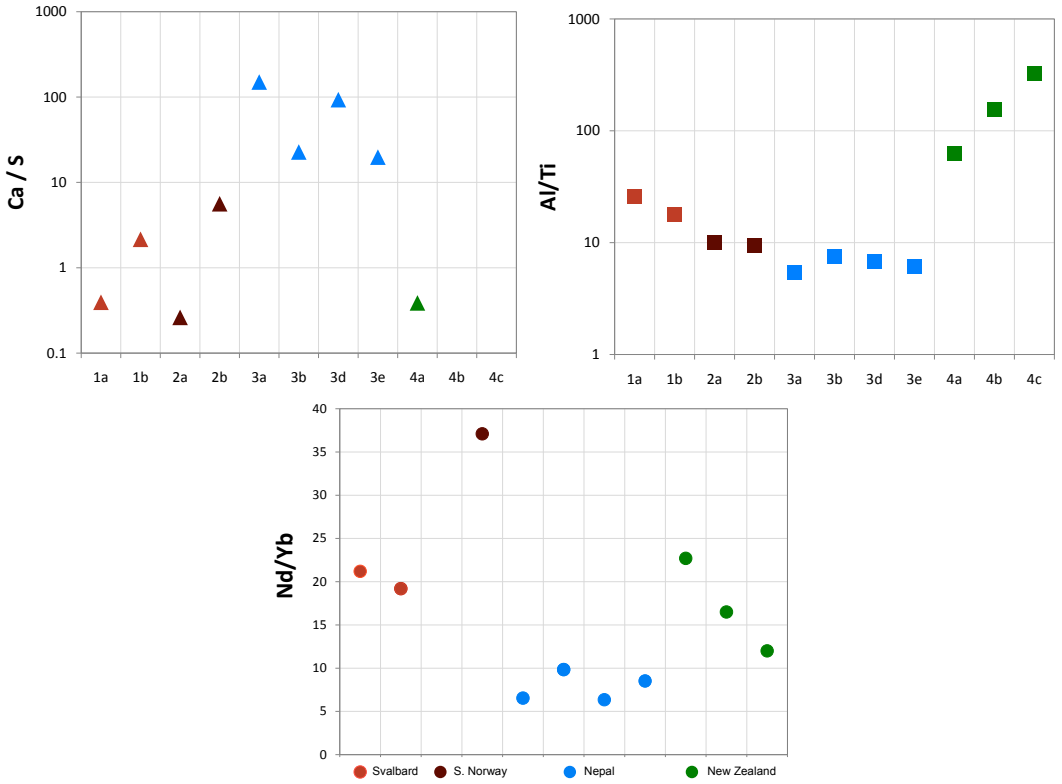

Fig. 5. Elemental ratio Ca/S, Al/Ti and Nd/Yb median value plots for snow and ice observations in each of the study regions, where the data points represent the following medians: Svalbard 1a, 1b; S. Norway 2b; Nepal 3a, 3b, 3d, 3e; New Zealand 4a, 4b, 4c). (Note, the Norway 2a, Nd/Yb Jostedalsbreen snow observation is not included due to Yb concentrations below instrumental detection limits. Also note the logarithmic scales in the Ca/S and Al/Ti plots.)

ESSDD
5, 107–145, 2012

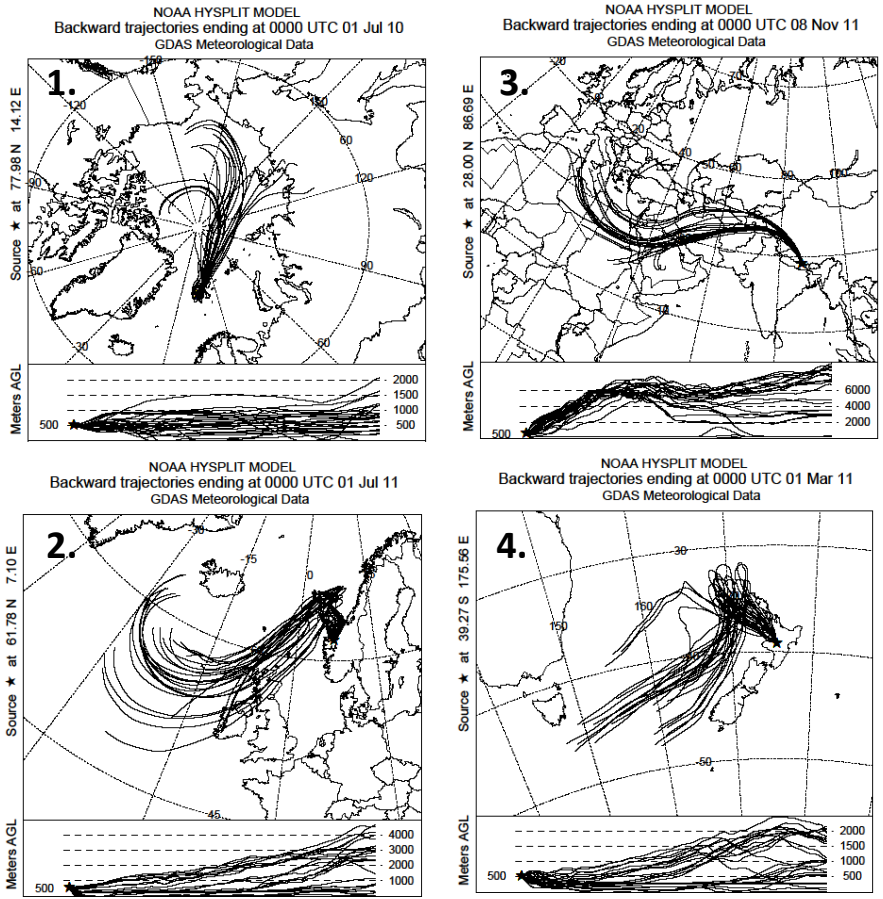

Fig. 6. NOAA HYSPLIT atmospheric 5-day transport trajectories for each glacier study region (1. Svalbard, 2. Norway, 3. Nepal, 4. New Zealand) using GDAS1 meteorology and 24 prediction trajectories.

ESSDD
5, 107–145, 2012